ADVANCED MATERIALS INTERFACES
www.advmatinterfaces.de

Nanostructured Ag-Bioglass Implant Coatings with Antibacterial and Osteogenic Activity

*Felix J. Geissel, Varvara Platania, Niccoló De Berardinis, Charlotte Skjöldebrand, Georgios N. Belibasakis, Cecilia Persson, Gry Hulsart-Billström, Maria Chatzinikolaidou, and Georgios A. Sotiriou**

Bone implant failure due to aseptic loosening and biofilm infections is an increasing healthcare problem. Implants may be coated with nanoparticles to avoid bacterial colonization and promote osseointegration. However, these nanocoatings often require long, expensive, and complex manufacturing routes with limited clinical translation potential. Here, a multifunctional nanoparticle coating consisting of silver (Ag) and bioglass (BG) is investigated to overcome current limitations by providing synchronously antibacterial and osteogenic effect. Flame spray pyrolysis (FSP) is exploited as a scalable and reproducible process to synthesize large quantities of nanoparticles and deposit them on titanium (Ti) substrates. The deposited nanocoatings show a homogeneous morphology and biomineralize after soaking in simulated body fluid (SBF), while their adhesion on Ti substrates is promoted by in situ flame annealing. The Ag^+ ion release from Ag containing BG samples inhibits *Staphylococcus aureus* biofilm formation up to 3 log units, while the osteogenic responses of pre-osteoblastic cells directly grown on AgBG samples show similar levels of alkaline phosphatase activity, calcium and collagen production when compared to pure Ti. The inexpensively synthesized multifunctional AgBG nanostructured implant coatings exert a high bioactivity and antibacterial response while maintaining high biocompatibility. The insights of this study can direct the development of multifunctional implant coatings.

1. Introduction

The increasing antimicrobial resistance to antibiotics and the ability of many microbes to form a biofilm may cause revision surgeries of infected implants.[1] During insertion of a medical device, bacteria may contaminate its surface and form a biofilm causing infection.[2] The administered antibiotics often cannot penetrate the biofilm and thus the only possibility left is to remove the implant and re-insert it. A successful bone implant should not only exert antibacterial properties, but also promote the integration with the host bone tissue (osseointegration[3]). Ideally, growth and differentiation factors initiate biological events which lead to new bone formation around the implant.[3] Without this bond to the bone, aseptic loosening can occur which leads to the failure of the implant. Ti implants exert already an improved biocompatibility compared to other metals due to the oxide layer which attracts fibroblasts and other vital cells for bone growth. However, there is still a need for superior materials since as of today around 10% of all implants fail.[4] This causes, in addition to huge financial costs to the healthcare system, significant psychological burden to the patients.[5]

Currently, these challenges are often tackled with various implant coatings. Metals and oxides are usually used to prevent early biofilm formation.[4] The osseointegration is usually attempted to be enhanced with bioactive glasses and calcium phosphate coatings.[6] Upon

F. J. Geissel, G. A. Sotiriou
Department of Microbiology
Tumor and Cell Biology
Karolinska Institutet
Stockholm 171 76, Sweden
E-mail: georgios.sotiriou@ki.se

V. Platania, M. Chatzinikolaidou
Department of Materials Science and Technology
University of Crete
Heraklion, Greece

N. De Berardinis, G. Hulsart-Billström
Department of Medicinal Chemistry
Uppsala University
Uppsala 751 05, Sweden

C. Skjöldebrand, C. Persson
Department of Materials Science and Engineering
Uppsala University
Uppsala, Sweden

G. N. Belibasakis
Division of Oral Diseases
Department of Dental Medicine
Karolinska Institutet
Stockholm 141 52, Sweden

M. Chatzinikolaidou
Institute of Electronic Structure and Laser (IESL)
Foundation for Research and Technology Hellas (FORTH)
Heraklion, Greece

The ORCID identification number(s) for the author(s) of this article can be found under https://doi.org/10.1002/admi.202201980.

DOI: 10.1002/admi.202201980

contact with biological fluids, those coatings can release ions, forming a hydroxyapatite (HA) layer on the implant's surface.[7] The HA chemical composition is very similar to the host bone tissue and thus promotes the osseointegration. Although coatings with antimicrobial and osseointegration properties have been investigated individually,[8,9] there are still several uncertainties when combining materials with these properties in the same coating. For example, most of those studies only benchmark their antibacterial properties with planktonic bacteria instead of biofilms, without demonstrating the potential application of such coatings on clinically relevant implant geometries.[10–12] Moreover, most nanomanufacture processes are not suitable for the large-scale production of such coatings which is important for their clinical translation.

Here, we produced multifunctional nanostructured coatings by flame aerosol nanoparticle direct deposition followed by in situ flame annealing on Ti substrates. With this scalable and reproducible nanomanufacture process, it is possible to fabricate homogeneous and multicomponent nanoparticle coatings on substrates with high control over nanoparticle size, coating thickness and composition. The coating consists of nanostructured BG and Ag nanoparticles (stated as *x*AgBG where *x* corresponds to the nominal Ag-content in wt% from 0 to 50 wt%). We performed a detailed characterization of the physicochemical and morphological properties of the as-deposited nanostructured coatings, and studied their antibiofilm activity in vitro against *S. aureus*, a prevalent pathogen found in implant infections.[13] Furthermore, the mechanical adhesion of the developed coatings was examined, and the bioactivity of the coatings was assessed by incubating the different samples with SBF. The formation of HA was analyzed with a scanning electron microscope (SEM), Fourier transform infrared spectroscopy (FTIR), and ion release kinetics. Moreover, their in vitro biocompatibility and proliferation was investigated, together with their osteogenic potential.

2. Experimental Section

2.1. Nanoparticle Coating Synthesis and Characterization

AgBG nanoparticles on Ti substrates (5 mm × 5 mm, Goodfellow) were deposited and the corresponding powder on a glass fiber filter (AlbetLabScience) with the aid of a vacuum pump (Busch) was collected. The liquid precursor consisted of the following complex stoichiometric concentrations: three final Ag contents (10, 20, and 50 wt%) were prepared with Ag acetate (Sigma, 99%) and mixed with 0.3 M of BG. This glass-composition was achieved with appropriate amounts of sodium 2-ethylhexanoic acid (2-EHA) (Sigma, 97%) calcium acetate hydrate (Sigma, ≥99%), hexamethyldisiloxane (Sigma, ≥98.5%) and tributyl phosphate (Sigma, ≥99%) dissolved in 2-EHA (Sigma, >99%) together with acetonitrile (Sigma, >99.8%,) and propionic acid (Sigma, ≥99.5%) at a final ratio 2:1:1.

This solution was then fed through a capillary with a syringe pump at a flow rate of 3 mL min^{-1} (New Era Pump Systems, Inc.) and out of 100 mL syringes (SGE Analytical Science) and was dispersed with 8 L min^{-1} flow rate of oxygen (>99.5%, AGA Gas AB) (EL-FLOW Select, Bronkhorst Ruurlo). A support flame of methane (1.5 L min^{-1} flow rate) and oxygen (3.2 L min^{-1} flow rate) ignited the fine mist (both gases >99.5%, AGA Gas AB). The Ti substrates were fixated onto a water-cooled holder over the nozzle at a distance of 10 cm. The deposition time was set to 120 s. Immediately after the deposition, all nanoparticle coatings were in situ annealed using an ethanol flame at distance 11 cm for 20 s.[14]

For particle characterization, transmission electron microscopy (TEM) was performed with a 120 kV LaB6 microscope Talos 120C G2 and a Ceta-D detector (Karolinska Institutet, 3D-EM facility). For preparation appropriate amounts of nanopowders were dispersed in ethanol with a sonicator. A droplet was then put on a copper grid and dried overnight before imaging. X-ray diffraction (XRD, Rigaku MiniFlex 600) determined the crystal structure of the as deposited coatings (since Ti shows a very distinct background pattern, the nanoparticles were deposited on Si substrates). The film morphology was evaluated with a scanning electron microscopy (SEM, Phenom Pharos, Thermo Fisher, and Gemini Ultra 55, Zeiss) The Ag^+ ion release in water (MiliQ) was measured with a sensitive electrode (Mettler & Toledo).

2.2. In Vitro Bioactivity

Two different nanosilver contents (x = 0 and 20 wt%) were immersed in SBF to investigate the ability to form a HA layer after certain time points. The 20AgBg was chosen due to its antibiofilm activity while keeping the Ag-content minimal. At 1, 3, 6, and 24 h the samples were taken out and gently rinsed with water. After a drying step all of them were examined with the SEM and FTIR (FTIR, ThermoFisher). In an additional step, the corresponding supernatant was filtered and diluted in nitric acid HNO_3 (1%) to measure the Ag, calcium, sodium, phosphorous and Si concentration with coupled plasma optical emission spectroscopy (ICP-OES, Avio 200, PerkinElmer).

2.3. Coating Adhesion Strength Evaluation

With a texture analyzer (TA) (Stable Micrometrics, UK) and a customized facet, the adhesion strength of the coating with the Ti substrate was measured. Samples without an annealing step (heat treatment) were compared to annealed ones. The 0AgBG was placed on a double-sided adhesive tape on the bottom pillar. After that the machine pushed a second pillar with an additional adhesive tape down and measured the force required to pull both apart. This force (or a translated weight) is the critical adhesion strength.

2.4. Antibiofilm Activity Against *S. aureus*

S. aureus (ATCC 25 923) was grown in tryptic soy broth (TSB) medium at 37 °C overnight and subsequently diluted to an optical density (OD) of 0.001 at 600 nm. This corresponds to around 8×10^5 bacteria. The four different samples were sterilized in an oven at 210 °C (Carbolite, Gero) and placed into a 48-well plate. Then an established biofilm growth protocol was

applied to incubate the samples together with the bacteria and assess their inhibition potential.[15]

2.5. In Vitro Biocompatibility of the Powders

All corresponding nanopowders were tested with the fibroblastic cell line L929 (ECACC General Collection, UK). Each sample consisted of a powder containing a progressive amount of Ag, expressed as a percentage by weight: (x = 0, 10, 20, and 50). The powders were sterilized at 200 °C for 3 h and dissolved in high-glucose DMEM medium (Gibco, USA) supplemented with 2 mM glutamine, 10% fetal bovine serum (FBS) (Sigma, USA) and 1% penicillin and streptomycin (pen-strep) (Gibco, USA). To help with the solubilization, the solution was sonicated for 1 h. Two concentrations for each sample were obtained, namely: 12.5 and 25 µg mL^{-1}. The two solutions were used to seed 5000 cells in each well of two separate 96-well plates (one for each concentration). Each group contained 6 repetitions. The cells were incubated in a sterile incubator at 37 °C with 5% of CO_2. After 48 h, the cell viability was quantitatively assessed using the resazurin-based metabolic assay AlamarBlue HS (Thermo Fisher, USA). Fluorescence measurements were obtained three times with a plate reader (CLARIOstar Plus, BMG Labtech, Germany) using an excitation wavelength of 560 nm and an emission wavelength of 590 nm and averaged. Three independent experiments were performed with the same setup and averaged.

2.6. In Vitro Biocompatibility of the Coatings

Pre-Osteoblastic Cell Culture Maintenance and Cell Seeding: Pre-osteoblastic cells MC3T3-E1 derived from the murine calvaria, were cultured in alpha-MEM minimum essential media (PAN Biotech, Germany), supplemented with 10% FBS (PAN Biotech, Germany), 100 units mL^{-1} of pen-strep, 100 mg mL^{-1} of streptomycin (PAN Biotech, Germany), 1% amphotericin (Gibco, USA). Cells between passages 8 to 10 were used for the experiments. Prior to cell seeding, the samples were immersed in culture media for 24 h to promote an Ag^+ ion burst release that is expected to affect the cell viability. The cell-loaded samples were maintained in a humidified atmosphere under 5% CO_2 at 37 °C and the culture media were changed twice a week. Tissue culture treated polystyrene (TCPS) was used as control surface.

Cell Viability and Proliferation Assay: The viability and proliferation of MC3T3-E1 pre-osteoblasts cultured in direct contact to the AgBG coated titanium samples was quantitatively assessed using the resazurin-based metabolic assay PrestoBlue (Invitrogen, USA) as previously described.[16] Briefly, the coatings were placed into 48-well plates and each sample was seeded with 10^4 cells. At each experimental time point of 3, 7, and 14 days of culture, the PrestoBlue reagent was added directly to the wells at a 1:10 dilution in culture medium and incubated at 37 °C for 60 min, before measuring the absorbance at 570 and 600 nm in a spectrophotometer (Synergy HT, Biotek, USA). The metabolic activity of living cells was correlated with the cell number by means of a calibration curve. All samples were analyzed in triplicates.

Cell Adhesion and Morphology Evaluation Via SEM: The adhesion and morphology of MC3T3-E1 pre-osteoblasts in direct contact with the coated samples was observed using SEM (JEOL JSM-6390 LV) after 14 days in culture. Seeded scaffolds with 10^4 cells per sample were placed in a CO_2 incubator at 37 °C for 14 days and then were removed from the incubator and rinsed three times with phosphate-buffered saline (PBS), fixed with 4% v/v paraformaldehyde for 20 min and dehydrated in increasing concentrations (30–100% v/v) of ethanol. The scaffolds were then dried in a critical point drier (Baltec CPD 030), sputter-coated with a 20 nm thick layer of gold (Baltec SCD 050) and observed under SEM at an accelerating voltage of 15 kV.

2.7. In Vitro Evaluation of Osteogenic Potential of the Coatings

Alkaline Phosphatase (ALP) Activity Measurement: An enzymatic activity assay was used to measure the levels of alkaline phosphatase activity expressed from the MC3T3-E1 cells cultured on the presence of the AgBG-coated Ti samples. Cells were cultured for 7, 14, 17, and 21 days in osteogenic medium, harvested at each time interval by trypsin-EDTA and collected by centrifugation. Pellets were dissolved in 100 µL lysis buffer (0.1% Triton X-100 in 50 mM Tris-HCl pH 10.5) and were subjected to two freeze-thaw cycles from –80 °C to room temperature. Then, 100 µL of a 2 mg mL^{-1} p-nitrophenyl phosphate (pNPP, Sigma, St. Louis, MO, USA) substrate in 50 mM Tris-HCl at pH 10 with 2 mM $MgCl_2$ were added to each sample and incubated at 37 °C for 60 min. The reaction was stopped with the addition of 50 µL 1 N NaOH. The absorbance was measured using a Synergy HTX plate reader (BioTek, Winooski, VT, USA) at 405 nm and was correlated to equivalent amounts of para-nitrophenol using a calibration curve.[17] The enzymatic activity was calculated using the equation [units = nmol p-nitrophenol min^{-1}] and normalized by the total protein. All samples were analyzed in triplicates.

Calcium Concentration Determination: Calcium deposition is a late marker for osteogenesis, signaling the formation of extracellular matrix (ECM) in bone tissue. The calcium using the O-cresol phthalein complexone (CPC) method was quantified. Supernatants were collected every 3 days up to day 21. 10 µL culture medium from each sample was mixed with 100 mL of calcium buffer (containing 1.7 mol L^{-1} amino-2-methyl-2-propanol-1 and 210 mmol L^{-1} hydrochloric acid) and 100 µL of calcium dye (containing 78 µmol L^{-1} O-cresol phthalein complexone (CPC), 3.36 mmol L^{-1} hydroxy-8-quinoline and 25 mmol L^{-1} hydrochloric acid). The final solutions were transferred in a 96-well plate and the absorbance was measured at 550 nm.[18] The absorbance measurements were correlated to the concentration of calcium using a calibration curve and normalized by the total protein. All samples were analyzed in triplicates.

Determination of the Produced Extracellular Collagen: The Sirius Red Dye assay (Direct red 80, Sigma-Aldrich, St. Louis, MO, USA) was used to measure total collagen levels secreted from the pre-osteoblastic cells in the culture medium. Briefly, at each time point, 25 µL of culture medium diluted in dd H_2O at a total volume of 100 µL and then mixed with 1 mL

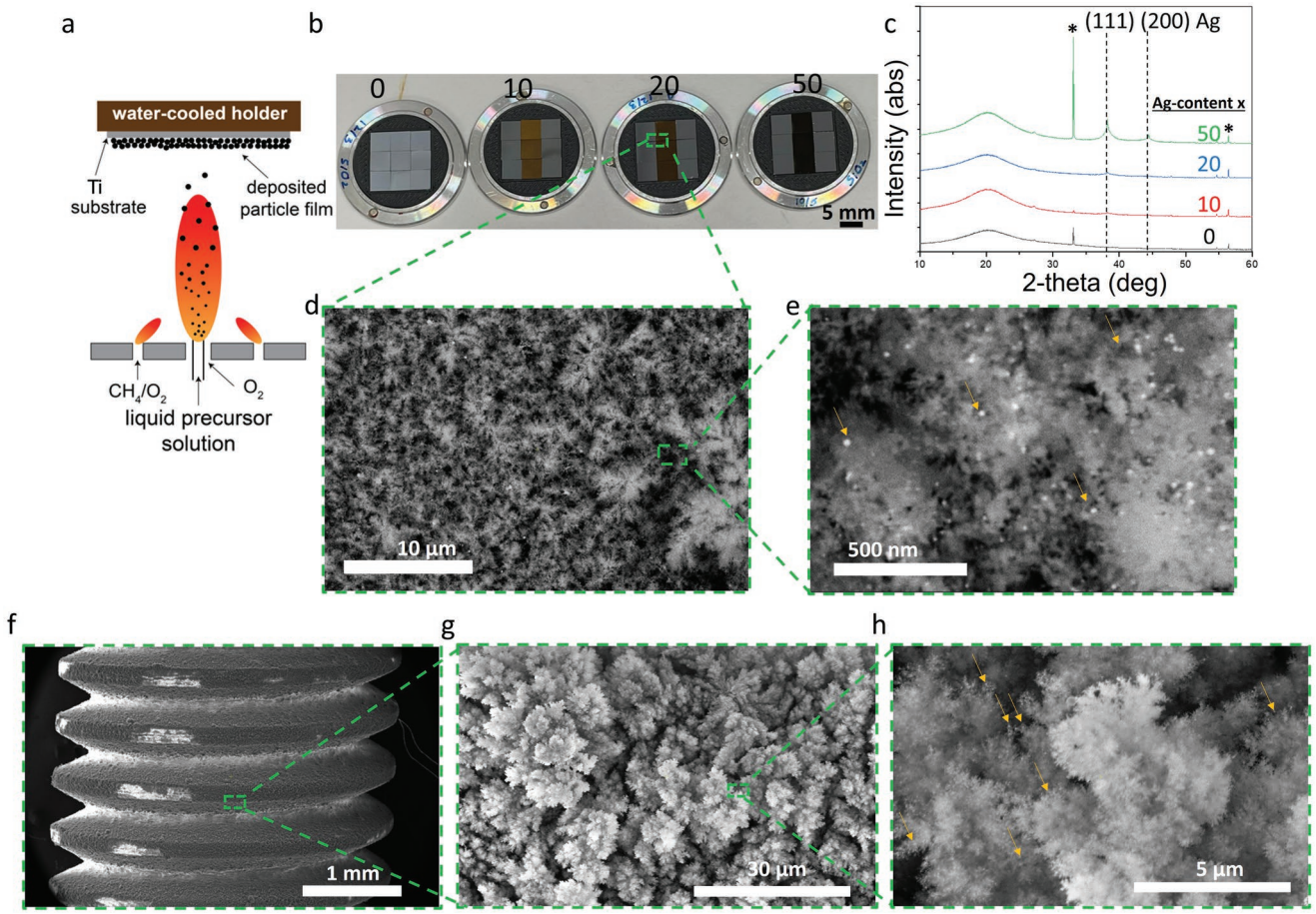

Figure 1. Flame aerosol direct nanoparticle deposition of multi-component AgBG nanoparticles. The deposited nanoparticle films, after their in situ flame annealing, retain their porous structure, while the deposition on complex 3D substrates is also possible. a) Schematic of the flame aerosol nanoparticle direct deposition process. b) Macroscopic view of the different samples (nanocoatings on the three Ti substrates in the middle: color change form bright to dark brown). c) Diffractogram of the coatings showing the characteristic (111) and (200) peaks of metal Ag. As the Ag-content increases the peak gets narrower suggesting bigger nanoparticles. d) SEM image of the 20AgBG showing the porous homogeneous structure and e) high magnification image where single Ag nanoparticles are visible (yellow arrows). SEM images f–h) at different magnification levels of the 50AgBG coating deposited on a screw.

0.1% Sirius Red Dye and incubated for 30 min at room temperature. After centrifugation of the samples at 15 000 *g* for 15 min, the pellets were washed with 0.1 N HCl in order to remove the non-bound dye. The samples were finally centrifuged at 15 000 *g* for 15 min and were dissolved in 500 µL 0.5 N NaOH. The absorbance was measured using a Synergy HTX plate reader at 530 nm.[19] The absorbance measurements were correlated to the concentration of collagen type I using a calibration curve and normalized by the total protein. All samples were analyzed in triplicates.

Statistical Analysis: The statistical analysis was performed in GraphPad Prism 9 (La Jolla, USA) using two-way ANOVA comparing the AgBG coatings to the control (pure Ti). For the in vitro cytotoxicity studies, the experimental data was analyzed using two-way ANOVA followed by Dunnett's multiple comparisons test between groups. The symbols designate as follows unless stated otherwise for an individual figure: $*p < 0.05$, $**p < 0.01$, n.s. = statistically non-significant difference compared to the pure Ti control surface.

3. Results and Discussion

3.1. Physicochemical and Morphological Characterization of the Coatings

FSP of a liquid precursor solution allows for nanoparticle production and deposition as a coating in a single step.[20] Ti substrates were herein coated with nanostructured films in this way, resulting in coatings consisting of composite xAgBG (Ag-content x = 0–50 wt%) nanoparticles, which were annealed in situ to increase the adhesion, cohesion, and structural stability.[14] **Figure 1**a shows an illustration of the FSP set-up with the direct deposition of the freshly formed nanoparticles as a coating on a water-cooled substrates through thermophoresis. Figure 1b shows images of all four samples with varying Ag-content (the three middle substrates among pure Ti substrates). As the Ag-content increases from 10 to 50 wt% the color changes from yellow to dark brown due to the plasmonic properties of nanosilver.[15] Figure 1c shows the XRD patterns of all

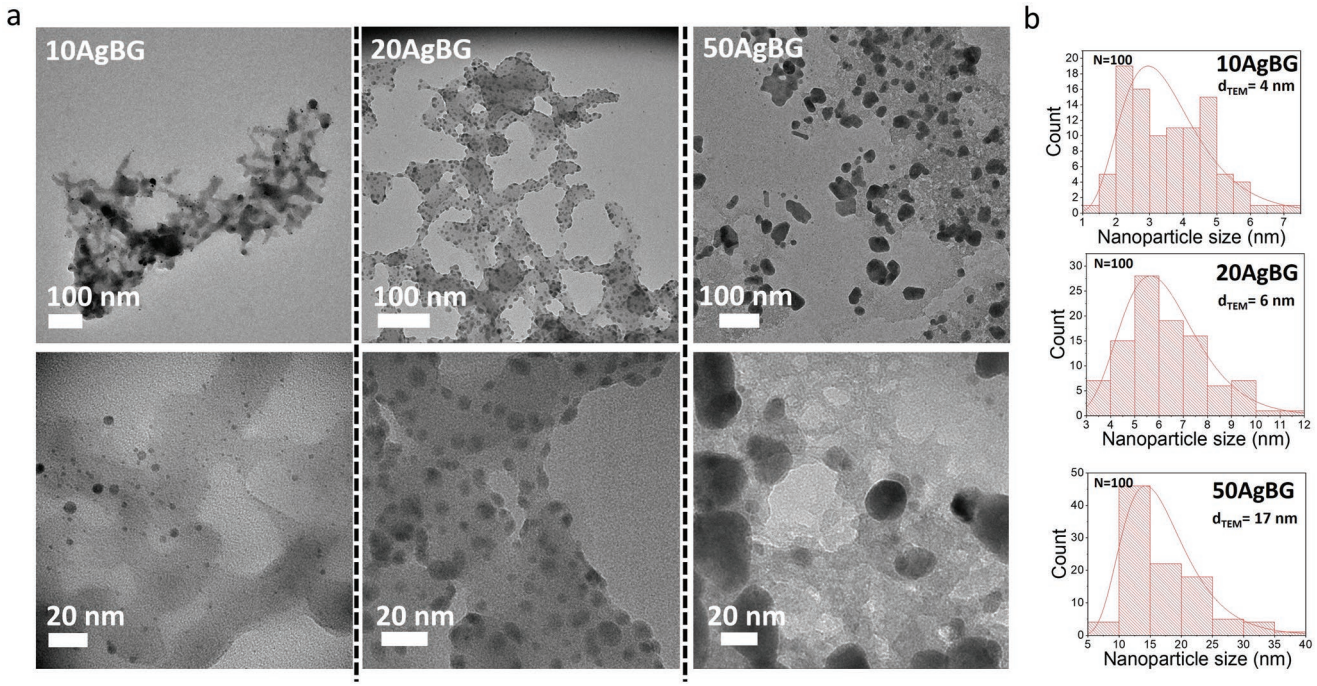

Figure 2. Morphological characterization and Ag nanoparticle size distributions by electron microscopy analysis. a) TEM images of the corresponding *x*AgBG powders of the three different Ag-contents ($x = 10$, 20, and 50 wt%). b) As the content increases the average nanoparticle size increases as well which is quantitatively shown in (b) along with the particle size distribution as well which shows the particle size distributions of the Ag nanoparticles.

coatings here highlighting the characteristic (111) peak of metal Ag (indicated with a dotted line). As the Ag-content increases, the main diffraction peak for Ag metal (111) becomes narrower indicating increasing crystal sizes. There is no evidence for Ag oxide formation,[21] or other crystal phase in the BG composition which indicates that it was formed without any crystalline structure. Therefore, the sharp peaks (highlighted by asterisks) are attributed to the silicon substrate (instead of Ti that exhibits several peaks and dominates the signal) used for the XRD analysis here.

To further examine the morphology of the deposited nanostructured coatings here, we performed SEM analysis as shown in Figure 1d,e. The coatings are homogeneous with high porosity, which is characteristic for their production method, and appear similar for all Ag-contents (Figure S1, Supporting Information). At high magnification (Figure 1e) some Ag nanoparticles can be observed for the 20AgBG sample (highlighted by yellow arrows). This morphology is similar to BG coatings in the literature.[22,23] To demonstrate the potential translation of flame direct deposition of particle coatings on relevant materials, 50AgBG coatings were deposited on a commercially available screw with geometry matching that of a bone screw for surgical fixation of hard tissue. Figure 1f–h shows the SEM images at three magnifications, demonstrating that the *x*AgBG coatings exhibit a homogeneous and porous morphology, similar to that of the flat Ti substrates. Depositing homogeneous coatings on complex geometries is a crucial step for further in vivo experiments or even clinical trials.

Figure 2a shows TEM images at two magnifications (top row: low magnification, bottom row: high magnification) of the different *x*AgBG samples ($x = 10$, 20, and 50 wt%) in their powder form (collected further downstream from the glass fiber filter). For all samples, the nanostructured aggregated BG support along with the presence of the Ag nanoparticles (shown dark here due to their high atomic number) is observed, in agreement with the literature for similar flame-made BG nanoparticles.[24] From all *x*AgBG samples, the Ag nanoparticles from the 20AgBG sample appear to be evenly dispersed on the amorphous BG support. For increasing Ag-content, the dispersed Ag nanoparticles are larger and more densely present in the composite nanoparticles. This is quantitatively validated by measuring the Ag particle size distribution from these TEM images (Figure 2b), verifying that the average nanoparticle size increases with increasing Ag-content from 4 to 17 nm, in agreement of the literature for flame-made Ag nanoparticles supported on inorganic material.[25–27]

3.2. In Vitro Bioactivity

Figure 3a shows SEM images taken of the 0AgBG (pure BG) and 20AgBG sample after soaking in SBF for 1, 3, 6, and 24 h. Conditioning BG in SBF results in the formation of a HA layer due to the ion release upon contact and the subsequent precipitation of that layer.[28] This HA layer enables the formation of a bond to the surrounding hard tissue and promotes osseointegration of the implant.[29] Indeed, for both coatings, a major film restructuring occurs resulting in the formation of a HA layer after 24 h (Figure S2, Supporting Information for additional SEM images). To better understand the HA formation, we acquired the FTIR spectra of these coatings for the different incubation times (Figure 3b,c) and measured their ion release

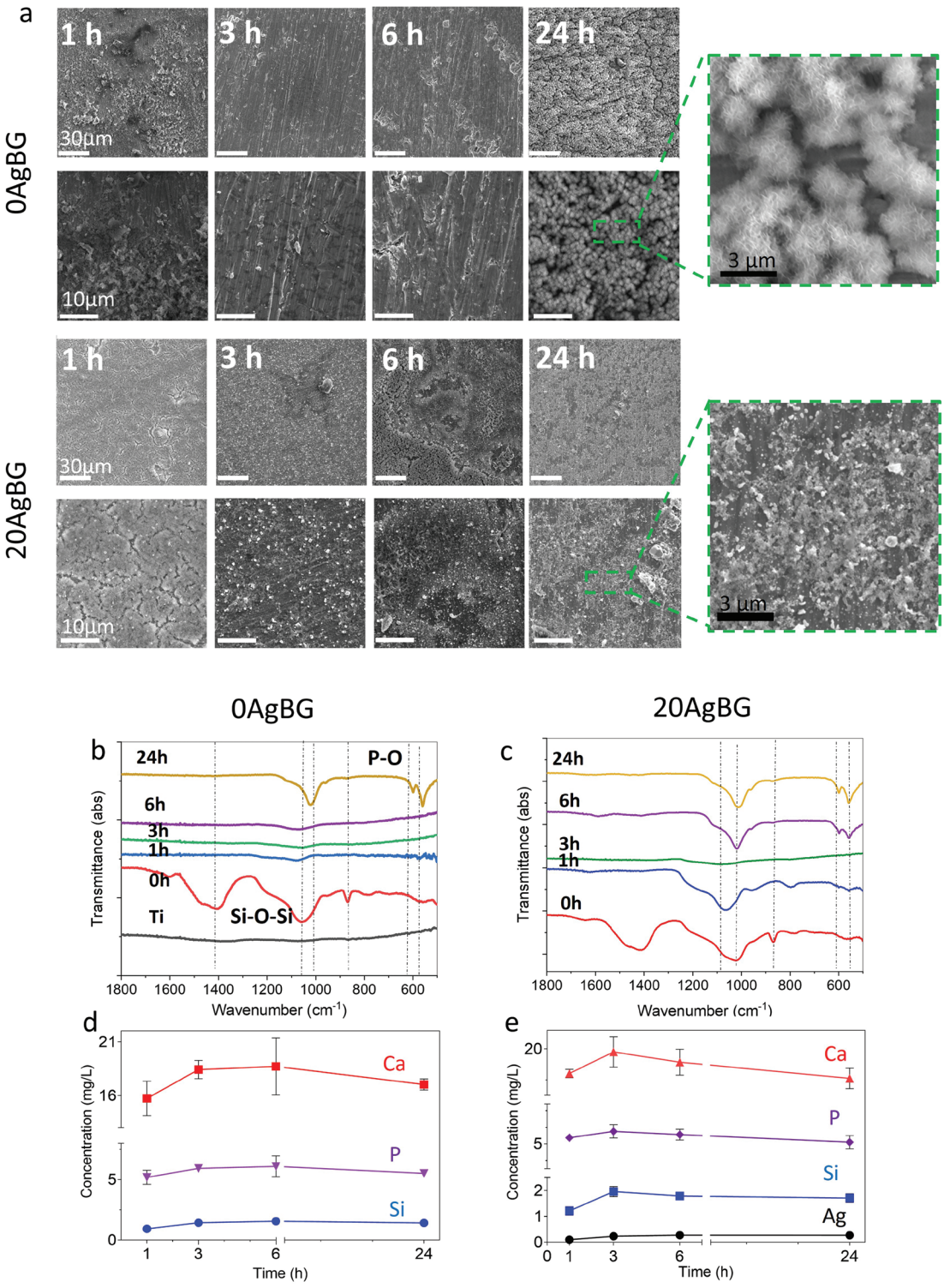

Figure 3. Electron microscopy analysis of the bioactivity of the pure BG and AgBG nanoparticle coatings upon their incubation in simulated body fluid (SBF). The formation of hydroxyapatite over time is validated by FTIR and elemental analysis of the supernatant. a) SEM images of 0AgBG (top part) and 20AgBG (bottom part) after various time points being incubated with SBF. FTIR spectra of b) 0AgBG and c) 20AgBG. The concentrations of the released elements in the supernatant from d) 0AgBG and e) 20AgBG, as measured by ICP-OES.

over time by ICP-OES (Figure 3d,e). The FTIR spectrum of the 0AgBG before any SBF incubation (Figure 3b, red line) exhibits bands attributed to Si–O$^-$– non-bridging oxygen (NBO$^-$) at ≈850 cm^{-1}, Si–O–Si stretching at ≈1100 cm^{-1} and SiOH bonding with molecularly absorbed water at ≈1450 cm^{-1}.[30] Upon incubation in SBF, there is first a decrease in the overall intensity

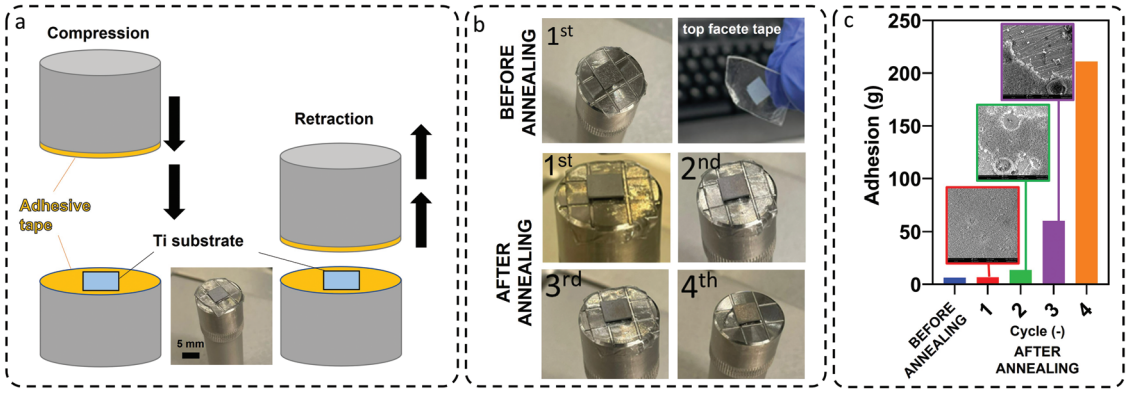

Figure 4. Mechanical characterization of the developed nanoparticle coatings. a) Schematic illustration of the adhesion testing using a TA. b) Images showing the 2 different conditions (before and after annealing) after the retraction. The coating of the sample without annealing is completely removed and sticks to the adhesive tape while the coating of the sample with annealing survives 3 cycles of increasing load. c) The adhesion of force of 0AgBG with SEM images as insets taken after the cycles.

indicating the dissolution and restructuring of the coating, and then at 24 h the characteristic bands of P–O stretch bonds attributed to the formation of HA. Similarly, the FTIR spectra of the 20AgBG exhibit these characteristic peaks, with the main difference being the faster coating restructuring to HA already appearing after 6 h.

Figure 3 also shows the respective supernatant concentrations of Si, P, Ca, and Ag (for Na ion release see Figure S3, Supporting Information) of the 0AgBG (d) and 20AgBG (e) over increasing incubation time in SBF. The presence of Ca, Na, and P in SBF renders the analysis of these elements difficult, but the increasing concentration of Si for both coatings (pure BG and 20AgBG) indicates partial dissolution from these coatings. For the pure BG coatings (Figure 3d) a slight increase also occurs also for P and Ca until 6 h which can be linked to the dissolution of the coating (Figure 3a). At 24 h these concentrations seem to drop indicating the HA layer formation since the elements precipitate from the supernatant toward the formation of HA.[31] For the 20AgBG sample (Figure 3e), however, a mild decrease of the Ca and P concentrations occurs already at 6 h instead of 24 h further supporting the FTIR data that shows the earlier formation of HA. Furthermore, the increasing concentrations of Ag over time in the case of the 20AgBG sample further validates its presence in these coatings and is in good agreement with the literature for other flame-made Ag-containing nanostructured coatings.[15]

3.3. Coating Adhesion before and after In Situ Flame Annealing

To evaluate the mechanical stability of the produced coatings, we performed an adhesion test utilizing a double-sided adhesive tape and mounting the Ti substrates on the customized facet of a TA (scheme in **Figure 4**a). Upon compression with an additional adhesive-coated facet to a defined constant force (8 N) and subsequent retraction, the coating is removed and the force necessary to pull up the facet is measured. A more mechanically stable coating would require more cycles (with new adhesive tape each time) of this compression–retraction process to be removed from the Ti substrate with increasing retraction force. Indeed, upon performing the compression–retraction process on a non-annealed coating, the coating is removed from the Ti substrate (Figure 4b) with a relatively low force required to pull up the compression facet (Figure 4c, please see Figures S4, Supporting Information for SEM images and Figure S5, Supporting Information for full force curves). In contrast, the in situ flame annealed coatings require at least four cycles to fully remove them from the Ti substrates (Figure 4b and Figure S6, Supporting Information for SEM images) with the increasing force necessary for each cycle (Figure 4c). This indicates that the in situ flame annealing improves the mechanical stability of these AgBG coatings, similar to other flame deposited coatings.[14] As insets in Figure 4c there are SEM images of the coatings after each compression–retraction cycle.

3.4. Antibiofilm Activity against *S. aureus*

The antibiofilm activity of the AgBG coatings was evaluated against *S. aureus* after their 24 h incubation in TSB medium at 37 °C with the bacterial suspension (OD_{600} = 0.001). **Figure 5**a shows a scheme describing the single steps of the experiment. **I)** The different samples are incubated with a bacterial solution for 24 h. **II)** After that they are gently washed to remove the planktonic bacteria which are not part of the early biofilm structure and kept in PBS. **III)** The early biofilm is recovered using a vortex/sonication step. **IV)** Serial dilutions are prepared and **V)** streaked out on agar plates. **VI)** On the following day the CFUs are counted. The Ag^+ ion release from the AgBG-containing coatings during the first hours inhibits the bacteria from their adhesion to the surface and consequently the formation of a biofilm.[32]

Figure 5b shows the CFUs mL^{-1} for the four different *x*AgBG coatings after rigorous washing by vortex/sonication.[15] On pure BG there is a high bacterial growth that gradually decreased with increasing Ag-content, reaching a 3-log CFUs mL^{-1} reduction at the highest Ag-content used (50AgBG). This antibiofilm activity is largely attributed to the released Ag^+ ions from the dissolution of the oxide layer on the nanosilver present in the

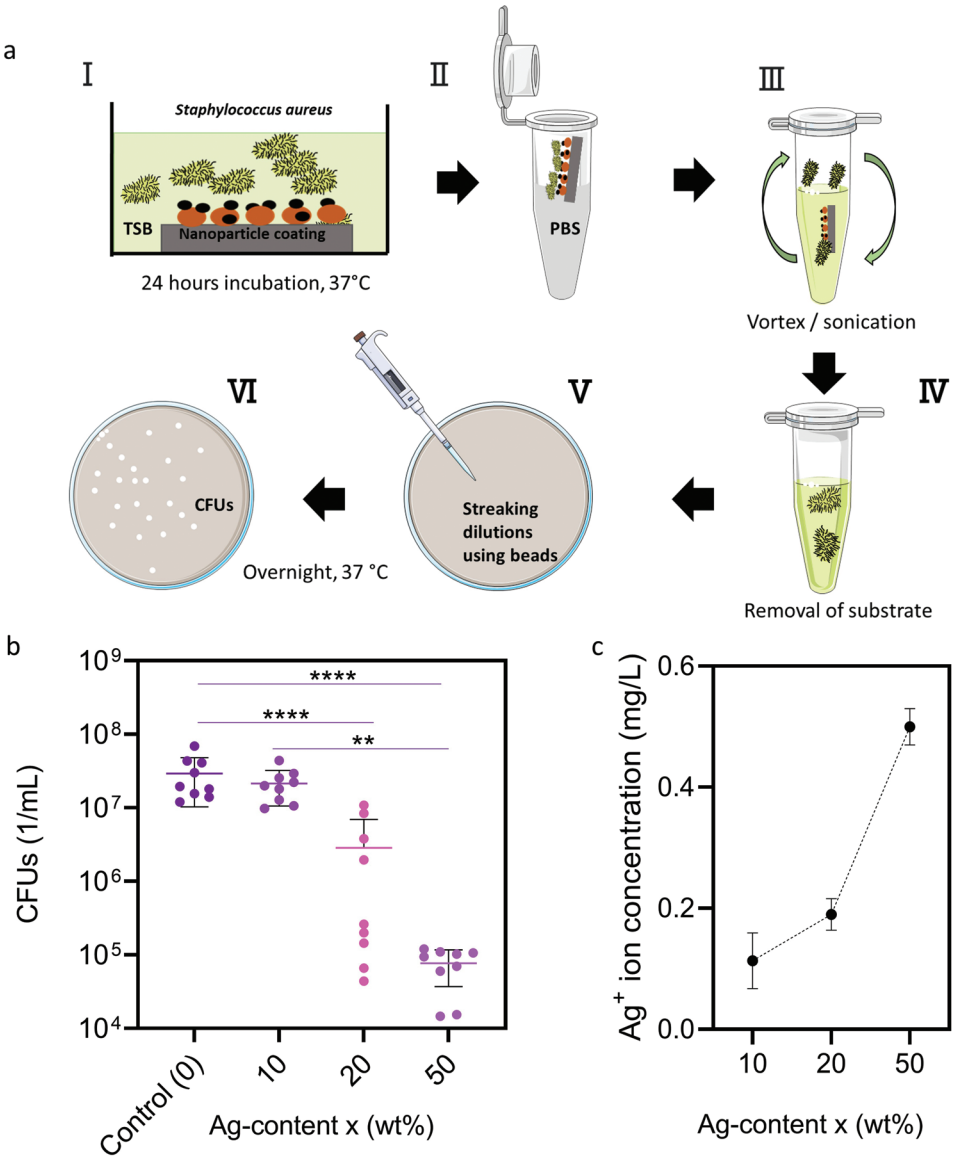

Figure 5. Biofilm growth experimental setup and biofilm inhibition results that are linked to the Ag+ ion release of the nanoparticle coatings. a) Scheme of the biofilm evaluation experiment. I) The coatings are covered with bacterial suspension and incubated for 24 h. II) Planktonic bacteria are removed with gentle washing in PBS. III) The biofilm is recovered with a sonication and vortex step. IV) Serial dilutions are prepared. V) The dilutions are spread using glass beads. VI) CFUs are counted. b) CFUs mL^{-1}-counts of retrieved bacteria after 24 h incubation with coatings from all Ag-contents compared to the untreated control (only BG nanoparticles). Each symbol represents the data obtained from the same technical replicate ($n = 9$). c) Ag^+ ion release from *x*AgBG coatings as a function of Ag-content *x* (10–50 wt%). For increasing ion release the CFUs mL^{-1} decrease for 3 log units. ****$p < 0.0001$.

*x*AgBG coatings.[15] The released Ag^+ ions can impair the biological function of bacteria by directly disrupting proteins functions, binding to DNA and by the production of reactive oxygen species that targets the cell envelope.[25,26,33–38] The CFU reduction on such Ag-based nanostructured substrates has also been validated by SEM analysis.[15] Similar outcomes are achieved by ECM degradation using bacteriophages and polysaccharides, however, those treatments are not surface based.[39] Indeed, Figure 5c shows the Ag^+ ion release after 24 h at 37 °C from the deposited coatings as a function of Ag-content upon their immersion into an aqueous solution. This release is similar to the immersion in TSB for the given experimental setup.[15] Therefore, the observed antibiofilm activity here is linked to the released Ag^+ ions from these coatings, in agreement with the literature.[15]

3.5. Biocompatibility and Osteogenic Capacity of the Coatings

The in vitro biocompatibility of all *x*AgBG samples was evaluated in both their powder form as well as coatings. The nanopowders were sterilized and then dispersed by sonication in DMEM medium. Subsequently, the solutions were used to culture the cells. Cell viability was monitored after 48 h with

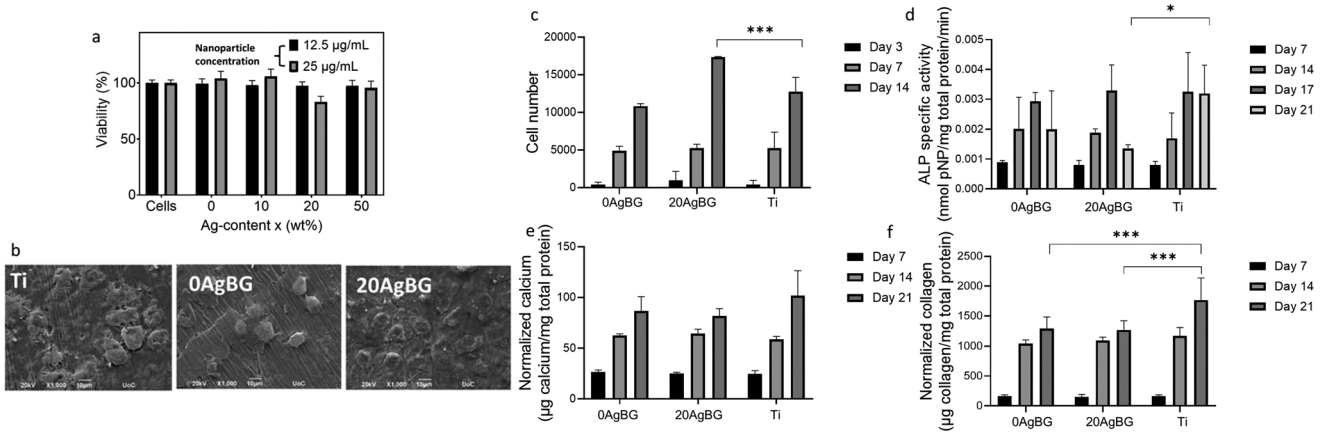

Figure 6. Biocompatibility assessment of the nanoparticles along with osteogenic biomarkers evaluation upon incubation with pre-osteoblasts. a) Cytotoxicity assessment of the four *x*AgBG powders (Ag-content x = 0–50 wt%) two concentrations (12.5 and 25 µg mL^{-1}) in pre-osteoblastic cells. b) SEM images of pre-osteoblast cells directly grown on the 0AgBG and 20AgBG coatings compared to cells grown on Ti (control) on Day 14. c) Cell viability and proliferation of pre-osteoblasts grown on pure BG (0AgBG), 20AgBG, pure Ti monitored over a period of 14 days. d) ALP activity, e) normalized calcium production, f) normalized collagen production from pre-osteoblasts grown on the surface of these substrates measured over 21 days.

the alamarBlue assay, as shown in **Figure 6**a. The nanoparticles do not exhibit any drastic decrease in cell viability for all Ag-contents at the low nanoparticle concentration of 12.5 µg mL^{-1}, while for increased nanoparticle concentration of 25 µg mL^{-1}, the viability is slightly reduced for both the 20AgBG and 50AgBG. This viability decrease in vitro has been observed for nanosilver-containing nanoparticles in the literature and is attributed to the released Ag^+ ions in solution.[27] This uncontrolled bioactivity of Ag^+ ions, that is also responsible for the antibacterial effect, constitutes a main limitation of nanosilver-containing coatings and thus an appropriate risk/benefit ratio needs to be established. Nonetheless, the observed high viability values here even for the Ag-containing nanoparticles indicate that the presence of BG in the composition of the nanoparticles might render these nanoparticles more biocompatible than when nanosilver is supported on pure amorphous SiO_2.[27,40]

The cell viability of MC3T3-E1 pre-osteoblastic cells cultured on the coatings is studied also with SEM imaging in Figure 6b. The coated substrates were preconditioned for 24 h in cell-free alpha-MEM to simulate the wound healing phase that starts days/weeks after the initial surgery,[41] and by when the released Ag^+ ions would have eliminated any bacteria and be depleted. This is especially important for implants susceptible to surface bacterial colonization where a quick local response is crucial.[42] Thus, Figure 6b shows the SEM images of three different samples (0AgBG and 20AgBG together with pure Ti as control) after 14 days incubation. The 20AgBG sample was chosen here for further analysis due to the highly dispersed Ag nanoparticles present on the BG support (Figure 2a). The cells have proliferated and are present on the surfaces with no major differences to the biocompatible Ti control.

Figure 6c depicts viability levels for the different samples (Ti substrate as a control, the 0AgBG and the 20AgBG nanostructured coatings) conducted with the PrestoBlue cell viability assay over 14 days. Most importantly, the cell number increases for all samples over time, indicating that the cells proliferate, and their population increases.[43] Furthermore, all samples exhibit lower viability than TCPS (data not shown), as expected, but when compared to Ti, the 0AgBG and 20AgBG coatings exhibit similar absorbances and hence no cytotoxicity. In the case of pure BG (0AgBG), the viability is even higher than the pure Ti substrate, further corroborating that the BG made here exhibits a rather biocompatible profile, in agreement with the literature.[44]

We further studied the osseointegration potential of the developed coatings. The ALP activity has been used as an early marker and the calcium deposition as a late marker to evaluate the effect of the coatings to the differentiation of the pre-osteoblasts to mature osteoblasts. Additionally, the secretion of the total collagen as the main structural component of the ECM was quantified, in order to investigate the potential of the pre-osteoblasts cultured on the coatings to promote ECM formation. Figure 6d depicts an increase of the ALP activity for both AgBG coatings in a comparable manner with no significant differences to the control Ti until day 17 followed by a steep decline at day 21 confirming their ability to induce early osteogenic differentiation of pre-osteoblasts. Regarding the calcium deposition (Figure 6e), both AgBG coatings demonstrate comparable values with the Ti control at all time points until day 21. Between the three time points, a linear increase in the calcium concentration is detectable, which implies that the pre-osteoblasts are constantly differentiating into osteoblasts up to day 21. Both the ALP activity and the calcium production results present a similar trend regarding the differentiation potential of the various AgBG coatings. As observed, the 20AgBG content does not seem to affect the overall osteogenic capacity promoted of the BG coatings. The deposition of type I collagen-rich ECM is a prerequisite for the expression of specific osteoblast products, such as the alkaline phosphatase, during the normal developmental sequence of the osteoblasts.[45] Collagen levels secreted by pre-osteoblasts on AgBG coatings demonstrate a threefold increase from day 7 to day 14 justifying the peak of ALP activity on day 17 (Figure 6f). These results suggest that the AgBG coatings support the ECM formation, which is

a crucial step required for the osteogenic differentiation. Even though here we study the osteogenic potential of these coatings by measuring several biomarkers with in vitro cell experiments with well-established methodology (see Table S1, Supporting Information for comparison to literature for osteogenic markers and techniques), further characterization by reverse transcription quantitative PCR and eventually in vivo animal models might offer additional insights. Nonetheless, the AgBG nanoparticle coatings developed here exhibit the well-known and desired osteogenic properties of common bioglass.[7]

4. Conclusion and Outlook

Here we synthesized composite nanostructuring AgBG coatings by flame aerosol direct deposition that allows for a facile control over the nanoparticle size and composition. This nanomanufacture process is highly scalable, reproducible and allows for the fabrication of nanostructured coatings on complex geometries facilitating their clinical translation. The mechanical adhesion of the developed coatings may be improved by an in situ annealing process, while simultaneously exhibiting bioactivity and biomineralization upon their incubation in SBF. These are very important characteristics to inhibit aseptic loosening and reduce implant failure by promoting osseointegration with the surrounding tissue. The antibiofilm activity of the developed coatings against *S. aureus*, a clinically relevant pathogen, was investigated and showed a high inhibition of up to 3-log units rendering it suitable to prevent implant infections. The cytotoxicity and biocompatibility of the developed multifunctional coatings were further studied in vitro with pre-osteoblasts, revealing that the AgBG coatings exhibit a similar osteogenic potential to pure BG demonstrating high ALP activity, calcium and collagen production. The results here provide the framework for the development of multifunctional coatings on medical implants to promote osseointegration and inhibit bacterial biofilm infections. Moreover, they add valuable knowledge for progressing toward in vivo studies and later into clinical trials.

Supporting Information

Supporting Information is available from the Wiley Online Library or from the author.

Acknowledgements

The authors kindly acknowledge the help of Vitalii Shtender with ICP-OES measuremnts and the following discussion of it. This project has received funding from the European Research Council (ERC) under the European Union's Horizon 2020 research and innovation program (ERC Grant Agreement No. 758705). Funding from the Karolinska Institutet Faculty Board, the Karolinska Institutet Strategic Research Stem Cells and Regenerative Medicine (StratRegen), the Swedish Research Council (Nos. 2021-05494, 2021-02059), and the Swedish Foundation for Strategic Research (Nos. FFL18-0043 and RMX18-0041) is kindly acknowledged. This research was also funded by the Hellenic Foundation for Research and Innovation (H.F.R.I.) under the "1st Call for H.F.R.I. Research Projects to support Faculty members and Researchers and the procurement of high-cost research equipment grant" (project number HFRI-FM17-1999). The authors thank Birgitta Henriques-Normark, Staffan Normark, and the BHN group (KI) for the insightful discussions.

Conflict of Interest

The authors declare no conflict of interest.

Data Availability Statement

The data that support the findings of this study are available from the corresponding author upon reasonable request.

Keywords

antibiofilm, bioglass, biomaterial, flame spray pyrolysis, multifunctional implant coating, nanosilver

Received: October 14, 2022
Revised: November 2, 2022
Published online: December 4, 2022

[1] H. Koo, R. N. Allan, R. P. Howlin, L. Hall-stoodley, P. Stoodley, *Nat. Rev. Microbiol.* **2018**, *15*, 740.
[2] C. R. Arciola, D. Campoccia, G. D. Ehrlich, L. Montanaro, *Adv. Exp. Med. Biol.* **2015**, *830*, 29.
[3] D. Apostu, O. Lucaciu, C. Berce, D. Lucaciu, D. Cosma, *J. Int. Med. Res.* **2018**, *46*, 2104.
[4] J. Raphel, M. Holodniy, S. B. Goodman, S. C. Heilshorn, *Biomaterials* **2016**, *84*, 301.
[5] S. Klouche, E. Sariali, P. Mamoudy, *Orthop. Traumatol. Surg. Res.* **2010**, *96*, 124.
[6] J. C. Vogt, G. Brandes, N. Ehlert, P. Behrens, I. Nolte, P. P. Mueller, T. Lenarz, M. Stieve, *J. Biomater. Appl.* **2009**, *24*, 175.
[7] F. Baino, S. Hamzehlou, S. Kargozar, *J. Funct. Biomater.* **2018**, *9*, 25.
[8] G. Xia, B. Song, J. Fang, *Research* **2022**, *2022*, 9896274.
[9] L. Liu, X. Pan, S. Liu, Y. Hu, D. Ma, *Smart Mater. Med.* **2021**, *2*, 302.
[10] K. Jurczyk, G. Adamek, M. M. Kubicka, J. Jakubowicz, M. Jurczyk, *Materials* **2015**, *8*, 1398.
[11] F. H. El-Batal, A. A. El-Kheshen, A. A. Abd El Aty, G. T. El-Bassyouni, *Silicon* **2018**, *10*, 1231.
[12] Y. Ding, Y. Hao, Z. Yuan, B. Tao, M. Chen, C. Lin, P. Liu, K. Cai, *Biomater. Sci.* **2020**, *8*, 1840.
[13] J. G. Bartlett, *Infect. Dis. Clin. Pract.* **2004**, *12*, 258.
[14] A. Tricoli, M. Graf, F. Mayer, S. Kühne, A. Hierlemann, S. E. Pratsinis, *Adv. Mater.* **2008**, *20*, 3005.
[15] F. J. Geissel, V. Platania, A. Gogos, I. K. Herrmann, G. N. Belibasakis, M. Chatzinikolaidou, G. A. Sotiriou, *J. Colloid Interface Sci.* **2022**, *608*, 3141.
[16] C. Hadjicharalambous, E. Mygdali, O. Prymak, A. Buyakov, S. Kulkov, M. Chatzinikolaidou, *J. Biomed. Mater. Res., Part A* **2015**, *103*, 3612.
[17] C. Hadjicharalambous, D. Kozlova, V. Sokolova, M. Epple, M. Chatzinikolaidou, *J. Biomed. Mater. Res., Part A* **2015**, *103*, 3834.
[18] K. Loukelis, D. Papadogianni, M. Chatzinikolaidou, *Int. J. Biol. Macromol.* **2022**, *209*, 1720.
[19] M. Chatzinikolaidou, C. Pontikoglou, K. Terzaki, M. Kaliva, A. Kalyva, E. Papadaki, M. Vamvakaki, M. Farsari, *Colloids Surf., B* **2017**, *149*, 233.

[20] A. Tricoli, M. Righettoni, S. E. Pratsinis, *Langmuir* **2009**, *25*,12578.
[21] S. Hannemann, J. D. Grunwaldt, F. Krumeich, P. Kappen, A. Baiker, *Appl. Surf. Sci.* **2006**, *252*, 7862.
[22] B. Tian, W. Chen, Y. Dong, J. v Marymont, Y. Lei, Q. Ke, Y. Guo, Z. Zhu, *RSC Adv.* **2016**, *6*, 8549.
[23] B. S. Necula, J. P. T. M. van Leeuwen, L. E. Fratila-Apachitei, S. A. J. Zaat, I. Apachitei, J. Duszczyk, *Acta Biomater.* **2012**, *8*, 4191.
[24] T. J. Brunner, R. N. Grass, W. J. Stark, *Chem. Commun.* **2006**, *13*, 1384.
[25] G. A. Sotiriou, S. E. Pratsinis, *Environ. Sci. Technol.* **2010**, *44*, 5649.
[26] G. A. Sotiriou, A. Teleki, A. Camenzind, F. Krumeich, A. Meyer, S. Panke, S. E. Pratsinis, *Chem. Eng. J.* **2011**, *170*, 547.
[27] A. Pratsinis, P. Hervella, J. C. Leroux, S. E. Pratsinis, G. A. Sotiriou, *Small* **2013**, *9*, 2576.
[28] A. Nommeots-Nomm, L. Hupa, D. Rohanová, D. S. Brauer, *Int. J. Appl. Glass Sci.* **2020**, *11*, 537.
[29] X. Wang, L. Yan, T. Ye, R. Cheng, J. Tian, C. Ma, Y. Wang, W. Cui, *Mater. Sci. Eng. C* **2019**, *102*, 415.
[30] J. Lao, X. Dieudonné, M. Benbakkar, É. Jallot, *J. Mater. Sci.* **2017**, *52*, 9129.
[31] G. Poologasundarampillai, B. Yu, O. Tsigkou, E. Valliant, S. Yue, P. D. Lee, R. W. Hamilton, M. M. Stevens, T. Kasuga, J. R. Jones, *Soft Matter* **2012**, *8*, 4822.
[32] J. Azeredo, N. F. Azevedo, R. Briandet, N. Cerca, T. Coenye, A. R. Costa, M. Desvaux, G. di Bonaventura, M. Hébraud, Z. Jaglic, M. Kačániová, S. Knøchel, A. Lourenço, F. Mergulhão, R. L. Meyer, G. Nychas, M. Simões, O. Tresse, C. Sternberg, *Crit. Rev. Microbiol.* **2017**, *43*, 313.
[33] G. A. Sotiriou, A. Meyer, J. T. N. Knijnenburg, S. Panke, S. E. Pratsinis, *Langmuir* **2012**, *28*, 15929.
[34] G. A. Sotiriou, S. E. Pratsinis, *Curr. Opin. Chem. Eng.* **2011**, *1*, 3.
[35] C. Gunawan, M. B. Faiz, R. Mann, S. R. S. Ting, G. A. Sotiriou, C. P. Marquis, R. Amal, *ACS Appl. Mater. Interfaces* **2020**, *12*, 5557.
[36] C. Gunawan, C. P. Marquis, R. Amal, G. A. Sotiriou, S. A. Rice, E. J. Harry, *ACS Nano* **2017**, *11*, 3438.
[37] M. B. Faiz, R. Amal, C. P. Marquis, E. J. Harry, G. A. Sotiriou, S. A. Rice, C. Gunawan, *Nanotoxicology* **2018**, *12*, 263.
[38] E. Valentin, A. L. Bottomley, G. S. Chilambi, E. J. Harry, R. Amal, G. A. Sotiriou, S. A. Rice, C. Gunawan, *Nanoscale* **2020**, *12*, 2384.
[39] N. M. C. Olsen, E. Thiran, T. Hasler, T. Vanzieleghem, G. N. Belibasakis, J. Mahillon, M. J. Loessner, M. Schmelcher, *Viruses* **2018**, *10*, 438.
[40] N. J. Hempel, P. Merkl, S. Asad, M. M. Knopp, R. Berthelsen, C. A. S. Bergström, A. Teleki, G. A. Sotiriou, K. Löbmann, *Mol. Pharmaceutics* **2021**, *18*, 2254.
[41] E. Öhnstedt, H. Lofton Tomenius, E. Vågesjö, M. Phillipson, *Expert Opin. Drug Discovery* **2019**, *14*, 485.
[42] P. Pallavicini, A. Taglietti, G. Dacarro, Y. A. Diaz-Fernandez, M. Galli, P. Grisoli, M. Patrini, G. Santucci De Magistris, R. Zanoni, *J. Colloid Interface Sci.* **2010**, *350*, 110.
[43] S. Tang, B. Tian, Y.-J. Guo, Z.-A. Zhu, Y.-P. Guo, *Surf. Coat. Technol.* **2014**, *251*, 210.
[44] B. Garrido, S. Dosta, I. G. Cano, *Bol. Soc. Esp. Ceram. Vidro* **2021**, *61*, 516.
[45] H. C. Blair, Q. C. Larrouture, Y. Li, H. Lin, D. Beer-Stoltz, L. Liu, R. S. Tuan, L. J. Robinson, P. H. Schlesinger, D. J. Nelson, *Tissue Eng., Part B* **2017**, *23*, 268.